Earthq Eng & Eng Vib (2013) 12: 165-184 **DOI**: 10.1007/s11803-013-0160-6

Site effects by generalized inversion technique using strong motion recordings of the 2008 Wenchuan earthquake

Ren Yefei[1†], Wen Ruizhi[1‡], Hiroaki Yamanaka[2‡] and Toshihide Kashima[3‡]

1. *Key Laboratory of Earthquake Engineering and Engineering Vibration, Institute of Engineering Mechanics, China Earthquake Administration, Harbin 150080, China*
2. *Tokyo Institute of Technology, Tokyo 226-8502, Japan*
3. *Building Research Institute, Tsukuba 305-0802, Japan*

Abstract: The generalized inversion of S-wave amplitude spectra from the free-field strong motion recordings of the China National Strong Motion Observation Network System (NSMONS) are used to evaluate the site effects in the Wenchuan area. In this regard, a total of 602 recordings from 96 aftershocks of the Wenchuan earthquake with magnitudes of *M*3.7–*M*6.5 were selected as a dataset. These recordings were obtained from 28 stations at a hypocenter distance ranging from 30 km to 150 km. The inversion results have been verified as reliable by comparing the site response at station 62WUD using the Generalized Inversion Technique (GIT) and the Standard Spectral Ratio method (SSR). For all 28 stations, the site predominant frequency F_p and the average site amplification in different frequency bands of 1.0–5.0 Hz, 5.0–10.0 Hz and 1.0–10.0 Hz have been calculated based on the inversion results. Compared with the results from the horizontal-to-vertical spectral ratio (HVSR) method, it shows that the HVSR method can reasonably estimate the site predominant frequency but underestimates the site amplification. The linear fitting between the average site amplification for each frequency band and the V_{s20} (the average uppermost-20 m shear wave velocity) shows good correlation. A distance measurement called the asperity distance D_{Aspt} is proposed to reasonably characterize the source-to-site distance for large earthquakes. Finally, the inversed site response is used to identify the soil nonlinearity in the main shock and aftershocks of Wenchuan earthquake. In ten of the 28 stations analyzed in the main shock, the soil behaved nonlinearly, where the ground motion level is apparently beyond a threshold of PGA > 300 cm/s^2 or PGV > 20 cm/s, and only one station coded 51SFB has evidence of soil nonlinear behavior in the aftershocks.

Keywords: generalized inversion technique; site effect; Wenchuan earthquake; soil nonlinearity; predominant frequency; site amplification

1 Introduction

It is generally believed that earthquake ground motions depend on the seismic source, path and site effect. It is widely recognized that the site effect is the most important characteristic of ground motion and has a strong impact on the earthquake damage. A typical case was observed in the 1985 Mexico earthquake, in which the soft-soil site significantly amplified the long-period ground motion leading to an unexpected vibration in distant high-rise buildings (Seed *et al*., 1988). In current engineering practice, consideration of the site effect is implemented by using different design response spectra for different site classes specified in seismic codes.

The earthquake magnitude determines the seismic motion at the source. The path effect, i.e., the seismic motion attenuation, is somewhat variable because of the stability of the crustal rock. However, the site effect is more flexible due to the anisotropic and heterogeneous characteristics of the site soil layers, and the irregular site topography, both of which are important research topics.

After the great Wenchuan earthquake, several studies were carried out on the site effects observed during the earthquake (Bo *et al*., 2009; Wang and Xie, 2010; Wen *et al*., 2010a; 2010b; Wen *et al*., 2011). However, these studies were restricted to a preliminarily qualitative description of the ground motion affected by different site conditions, and do not include a quantitative evaluation. It is expected that an accurate site response may be calculated based on the propagation theory of seismic waves. However, in reality, it is usually difficult to obtain the exact geotechnical data of deep crust media, and it is also difficult to model the anisotropic and heterogeneous of the media. Another reason is

Correspondence to: Wen Ruizhi, Institute of Engineering Mechanics, China Earthquake Administration, Harbin 150080, China
Tel: +86-451-86652617; Fax: +86-451-8666475
E-mail: ruizhi@iem.net.cn
†Research Assistant; ‡Professor

Supported by: Nonprofit Industry Research Project of CEA under Grant No. 201208014; National Natural Science Fund No. 51278473; Environmental Protection Research Fund for Public Interest No. 201209040
Received February 7, 2013; **Accepted** May 6, 2013

that the 3-D physical model of soil nonlinearity in the case of large strain is very complicated and still not well understood. Therefore, there are some widely adopted methods that use the strong motion recordings to inverse site response, such as the Standard Spectral Ratio method (SSR) (Borcherdt, 1970), the Horizontal-to-Vertical Spectral Ratio method (HVSR) (Field and Jacob, 1995) and the Generalized Inversion Technique (GIT) (Andrews, 1986), which is used in this study. The benefit of GIT is that it can separate the source, path and site effect.

Furthermore, it is fortunate that a large number of strong motion recordings were obtained from the Wenchuan main shock and aftershocks, which made this study possible. The National Strong Motion Observation Network System (NSMONS) of China started formal operation in March 2008, just two months before the Wenchuan earthquake (Li *et al*., 2008). More than 400 sets of 3-channel recordings were accumulated in the main shock and more than 2000 sets were acquired from 383 aftershocks (Li, 2009). In this study, the site response of some strong motion stations around the Wenchuan area is inversed. Then, correlation of the site amplification with the surface geology is discussed. The predominant frequency and average site amplification of each station is evaluated. Finally, the inversed site response at each station is utilized to identify the soil nonlinearity in the main shock and aftershocks separately.

2 Methodology

2.1 Generalized inversion technique

The GIT used in this study, which is also called the Spectral Inversion Method (SIM) in some of the literature was first proposed by Andrews (1986). The advantage of this method is that it can separate the terms of source, path and site effect of the observed ground motions. Andrews (1986) assumed that every observed power spectrum is the product of a station-response spectrum and an event spectrum. However, it only considers the geometrical spreading factor for path term. Therefore, Iwata and Irikura (1986, 1988) made a further improvement by adding another important factor, the inelastic losses of ground motion, into the path term.

Since then, the GIT has been widely applied by many engineers and scientists, and was used to evaluate the site characteristics in most studies, e.g., Hartzell (1992); Harmsen (1997); Dutta *et al*. (2001); Salazar *et al*. (2007); Drouet *et al*. (2008); Tsuda *et al*. (2010), etc. Another popular application of the GIT is to estimate the source parameters (Iwata and Irikura, 1988; Fletcher and Boatwright, 1991; Moya *et al*., 2000; Dutta *et al*., 2003). Moya *et al*. (2000) used genetic algorithms (GA) to improve this method in order to estimate the most stable site effect with an assumption of a ω^2 source model (Brune, 1970 and 1971) for each earthquake. As an example, they used the improved method to reasonably estimate the source parameters for the aftershocks of the 1995 Kobe earthquake. Some other applications of this method include evaluating the Q value of either S wave or P wave (Hasemi *et al*., 1997), researching the effect of rupture directivity on ground motion (Hoshiba, 2003), researching the topographic effect on ground motion (Francisco *et al*., 1997), identifying the soil nonlinearity behavior for strong ground motions (Takemura *et al*., 1991; Field *et al*., 1997, 1998), and comparing and verifying the results of site effect by the SSR method and HVSR method (Field and Jacob, 1995; Parolai *et al*., 2004).

It has been believed that ground motion in the far field is described as a convolution of source, path and site factors. In the frequency domain, the observed spectrum of an earthquake can be expressed as a linear multiplication of these three factors:

$$O_{ij}(f) = S_i(f) \cdot P_{ij}(f) \cdot G_j(f) \tag{1}$$

where $O_{ij}(f)$ is the observed spectrum of the ith earthquake at the jth station, $S_i(f)$ is the source of the ith earthquake, $P_{ij}(f)$ represents the path effect, i.e., the attenuation of the ground motion, and $G_j(f)$ is the site effect at the jth station.

The path effect includes two factors that assume the earthquake source as a point: one is the geometric spreading which can be expressed in terms of R_{ij}^{-1}, and the other is the inelastic losses. Then, the path term $P_{ij}(f)$ can be represented as follows:

$$P_{ij}(f) = R_{ij}^{-1} \cdot \exp(-\pi f R_{ij}/Q(f) \cdot V_{\mathrm{s}}) \tag{2}$$

where R_{ij} is the hypocenter distance from the ith source to the jth station, $Q(f)$ is the frequency- dependent quality factor, and V_{s} is the shear wave velocity of the medium. Then, the observed spectrum would be represented as

$$O_{ij}(f) = S_i(f) \cdot G_j(f) \cdot R_{ij}^{-1} \cdot \exp(-\pi f R_{ij}/Q(f) \cdot V_{\mathrm{s}}) \tag{3}$$

Performing a logarithmic operation, the Eq. (3) will become a form of linear sum:

$$\ln(O_{ij}(f)) + \ln R_{ij} = \ln(S_i(f)) + \ln(G_j(f)) - (\pi f R_{ij}/V_{\mathrm{s}}) \cdot Q(f) \tag{4}$$

Equation (4) can be written in a matrix form:

$$\boldsymbol{Ax} = \boldsymbol{b} \tag{5}$$

where $\boldsymbol{A}$ is the sparse matrix containing three nonzero elements in each row (two 1 and $-\pi f R_{ij}/V_{\mathrm{s}}$). $\boldsymbol{x}$ represents a solution vector consisting of the unknown parameters of the terms on the right side of Eq. (4), and $\boldsymbol{b}$ is the term on the left side written as a vector, which is already given.

Equation (5) can be solved by using the singular value decomposition method (Lawson and Hanson, 1974). However, there are I (source spectrum) + J (site effect) + 1 (Q value) unknown parameters determined by $I \times J$ equations at each frequency, which means that an unconstrained degree of freedom exists in this system. It poses a trade-off between source and site effect. To remove it, a constraint condition should be given by choosing at least one reference site or event. Usually for simplicity many authors prefer to use a rock site as a reference site, and then set the site effect $G_{ref}(f) = 1$ at each frequency (e.g., Field and Jacob, 1995; Francisco *et al*., 1997; Parolai *et al*., 2004; Matsunami *et al*., 2003; Dutta *et al*., 2003). Others use the same assumption but set $G_{ref}(f) = 2$ to consider the free surface amplification (e.g. Iwata and Irikura, 1988; Takemura *et al*., 1991; Kato *et al*., 1992).

However, in real cases, the very hard-rock reference site is difficult to find. Sometimes even the hard-rock site has its own frequency-dependent amplification (Shoji and Kamiyama, 2002; Moya *et al*., 2000). Perhaps the thin weathering surface layer causes site amplification at high frequencies (Yoshimoto *et al*., 1993; Steidl *et al*., 1996). Thus, Hassani *et al*. (2011) used $G_{ref}(f)$ value of the rock site given by Boore and Joyner (1997), which used the quarter-wavelength method to evaluate site amplification of a generic rock site.

Sometimes the topography around the reference site also has a significant effect on the site amplification (Kato *et al*., 1992). To obtain an accurate and reasonable result, the site effect of the reference site was calculated numerically by using detailed geotechnical data (Yamanaka *et al*., 1998; 2011).

In addition, some researchers chose a reference event as a constraint condition by constraining its source spectrum $S_{ref}(f)$. Boatwright *et al*. (1991) and Fletcher and Boatwright (1991) proposed this technique initially when using a two-step iterative inversion for moderate-sized earthquakes. Moya and Irikura (2003) used the given seismic moment and corner frequency for a reference event by following the ω^2 model to constrain the shape of its source. Then, the spectral ratios between stations were estimated in order to remove the source terms so that the number of unknowns is limited to the number of sites and the Q factor.

2.2 Constraint condition in this study

In the present study, a strong motion station coded 62WIX is selected as a reference site, and a site response of $G_{ref}(f) = 2$ is assumed for the entire frequency range considering the free surface amplification. Even though the amplification as discussed above also exists at high frequency for the hard-rock site, it is still assumed that there is no site response for this site. In fact, it belongs to the China Earthquake Networks Center (CENC). A broadband seismometer was also installed on this station. The foremost primary requirement for this type of measurement is indispensable at very low ambient vibration. Thus, it is better to install all the sensors, including the accelerometer, inside a cave in the mountain. Figure 1 shows an outside view of the 62WIX Station. It is apparent that the site can be seen as outcrop without weathered layer coverage and the site response can be neglected. The calculated Fourier spectrum *H/V* ratio of the S-waves of the strong motion recordings obtained at this station during the aftershocks of the Wenchuan earthquake is shown in Fig. 2. Note that there is no obvious predominant frequency and the ratio value almost equals to unit, which supports the assumption of no site response for this site.

Fig. 1 Photo of the entrance of 62WIX Station

To further investigate the existence of the free surface amplification, the distance from the surface to the cave is measured. The measured value is satisfactory as it is only about 10 m–20 m, as shown in Fig. 3. In addition, the topographic effect at this site is also considered via a roughly visual identification. From Fig. 3, it can be seen that the absolute elevation of the mountain where Station 62WIX is located is not very high, only 180 m. The station is located on a very gentle slope and is much closer to the bottom rather than the top. This leads to the conclusion that it is reasonable to neglect the topographic effect at Station 62WIX.

3 Dataset and data processing

3.1 Dataset

A large number of strong motion recordings were

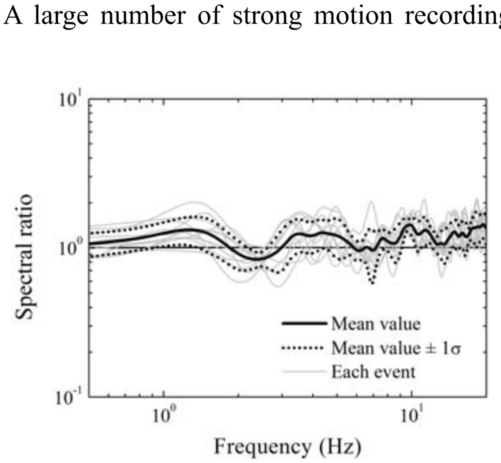

Fig. 2 Fourier spectrum *H/V* ratio of the strong motion recordings at the Station 62WIX

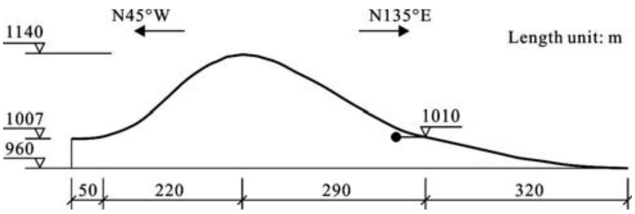

Fig. 3 Sketch of the topography of the Station 62WIX

acquired, which makes it possible to select appropriate data to use for the inversion. The selection criteria are shown in Fig. 4 and the details are listed below.

(1) Considering the fact that the ground motion attenuation is dependent on the magnitude and distance, in this study the hypocenter distance of selected recordings is limited to 30 – 150 km. Most of the recordings are kept in this range in order to achieve a relatively uniform distribution. Another reason is that the geometric spreading function is assumed as R_{ij}^{-1} in this study, which is not suitable for very far-field sites.

The error of focal depth will affect the hypocenter distance calculation for near-field sites. All aftershocks of the Wenchuan earthquake belong to the shallow-source type and the maximum focal depth is 30 km for all events in which strong motion recordings are provided, so the value of 30 km is defined as the lower limit of the hypocenter distance.

(2) The average PGA of two horizontal components should be larger than 2 cm/s^2 and less than 100 cm/s^2.

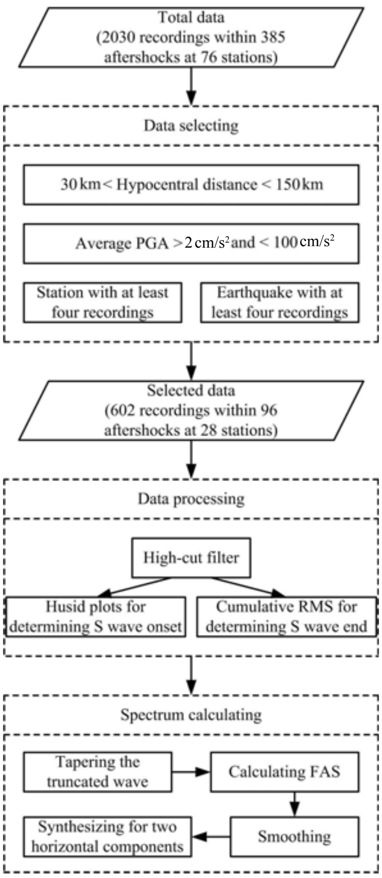

Fig. 4 Flowchart of data selecting and processing

The lower-limit value is assigned to avoid contamination of the recording by the noise. And, the upper-limit value is set to avoid the effect of site soil nonlinearity. To consider the possibility of site soil nonlinearity, many studies specified some different threshold peak acceleration values, such as 100–200 cm/s^2 (Beresnev and Wen, 1996), 150–200 cm/s^2 (Beresnev *et al.*, 1998), 200–300 cm/s^2 (Hartzell, 1998; Roumelioti and Beresnev, 2003), and 300 cm/s^2 (Su *et al.*, 1998). Here the value of 100 cm/s^2 is chosen to minimize the effect of soil nonlinearity.

(3) To ensure scattering of the inversion results will be at a relatively low level, each event selected should be recorded by at least four stations, each of which should provide at least four recordings that match Criteria (1) and (2).

Finally, 602 recordings from 96 aftershocks at 28 stations make up a dataset for inversion analysis. Figure 5 shows the geographical distribution of the earthquake epicenter and the station location. Figure 6 shows the magnitude-distance and magnitude-PGA distribution of these recordings. From the left side of Fig. 6, it is seen that the hypocenter distance has a uniform distribution in the range of 30 – 150 km. The list of earthquake information containing the event ID, epicenter location, focal depth, magnitude and number of recordings is provided in Appendix A, and the list of station information containing the Station ID, geographical coordinates, number of recordings and V_{s20} (average shear wave velocity of 20 m-thickness soil overburden) is presented in Appendix B.

3.2 Data processing

For data processing, first a 25 Hz high-cut filtering is

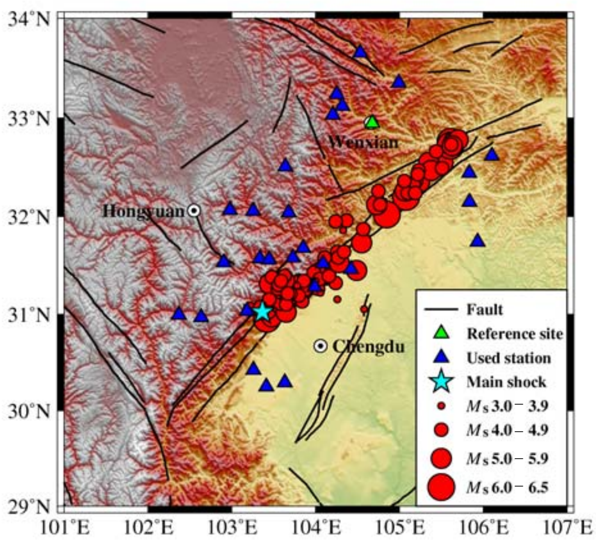

Fig. 5 Epicenter location of the earthquakes and geographical distribution of strong motion stations used in this study. The reference Site 62WIX is marked by a green triangle

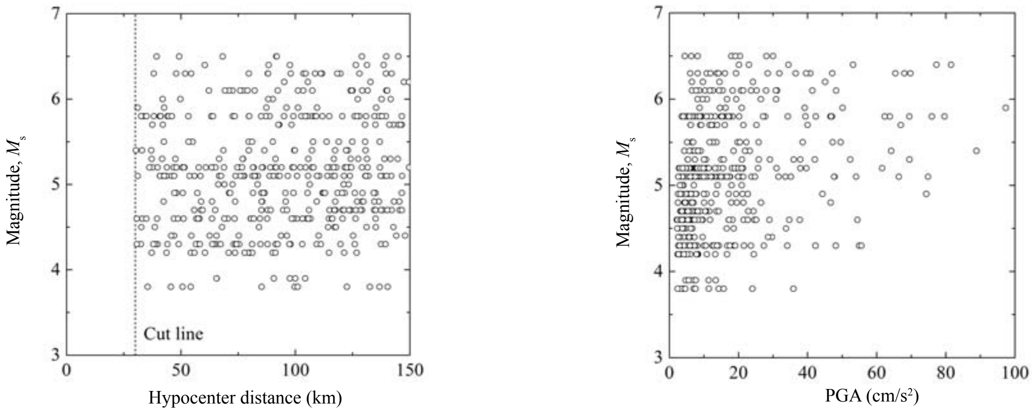

Fig. 6 Magnitude-distance and magnitude-PGA distribution of recordings used in this study. The cut line means the lower-limit value of 30km

performed to remove the high-frequency noise. In fact, above 25 Hz, high-frequency noise does not affect the frequency band of 0.5–20 Hz interested in this study, but it may make it difficult to detect the S wave portion.

The onset of the S wave arrival time is identified by Husid plot which shows the buildup of the energy of an accelerogram with time (Husid, 1967). If using $a(t)$ as the expression of acceleration time-series, the Husid plot $H_n(t)$ will be given by:

$$H_n(t) = \frac{\int_0^t [a(t)]^2 \,\mathrm{d}t}{\int_0^\infty [a(t)]^2 \,\mathrm{d}t} \tag{6}$$

The end instant of the S wave is detected by using the cumulative Root Mean Square (RMS) function (McCann and Shah, 1979) as follows:

$$\mathrm{CRMS} = \sqrt{\frac{1}{T}\int_0^T \|a(t)\|^2 \,\mathrm{d}t} \tag{7}$$

where $a(t)$ denotes the time-series, and T denotes the computed duration.

In this study, the end instant of the S wave is defined as the starting point of the decreasing tendency of the cumulative RMS curve along with the time. This technique had been applied in the study of Hassani *et al.* (2011) as well. To remove the truncated error, a cosine-type tapered window is used, as shown in Fig. 7. Before the onset and after the end of the S wave, a time-series with a duration corresponding to 10% of the S wave is added to the S wave portion to run the tapering. To reduce the effect of the contamination of the surface wave as far as possible, when the duration of the S wave is larger than 12 s, it will be set as 12 s according to the maximum magnitude in the dataset, which is $M_s 6.5$.

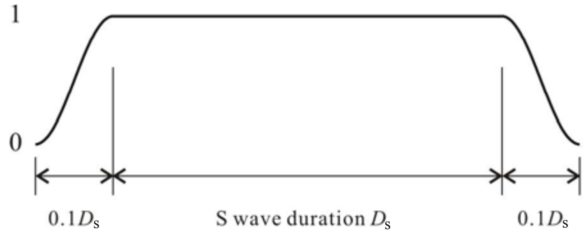

Fig. 7 Tapered function used in the present study

Figure 7 shows a demonstration of how the onset and the end of the S wave are automatically identified. Following the flowchart of data processing shown in Fig. 4, after obtaining the S wave portion, the Fourier Amplitude Spectrum (FAS) for each horizontal component is calculated. Then a 0.5 Hz-width Parzen window is used to smooth the spectrum. Finally, the resulting horizontal FAS $H(f)$ is vectorially synthesized by Eq. (8), where $H_1(f)$ and $H_2(f)$ represent the FAS of two orthogonal components.

$$H(f) = \sqrt{H_1^2(f) + H_2^2(f)} \tag{8}$$

4 Results and discussions

4.1 Verification of the reliability of the inversion calculation

To verify the accuracy and reliability of the inversion calculation, two adjacent stations are selected to compare

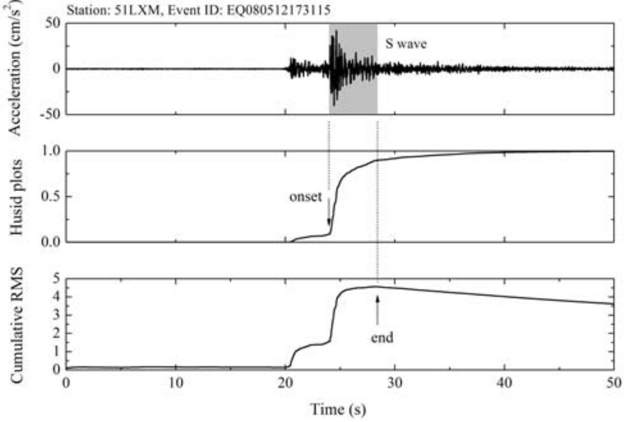

Fig. 8 Demonstration for the automatically identifying onset and end of S wave in the present study. The upper figure shows the waveform, the middle shows the Husid plots and the lower shows the cumulative RMS

the inversion result with the observed result by the SSR method (Borcherdt, 1970). As previously discussed, the reference Station 62WIX is outcrop without any weathered layer coverage, and Station 62WUD is used as the analyzing station, which is recognized as a very soft site with V_{s30} equal to 221 m/s (Wen *et al*., 2011). Five events with similar hypocenter distance of these two stations are obtained, of which the basic information is given in Table 1. Figure 9 shows the locations of both stations and earthquake epicenter.

Due to the same earthquake source and similar hypocenter distance for these two stations, the terms of source and path effect can be ignored as shown in Eq. (9). Therefore, the ratio of the observed Fourier amplitude spectra of the two stations can be identical to the ratio of site responses. In Eq. (9), a subscript ref represents the reference site.

$$\frac{O_{ij}(f)}{O_{i,\mathrm{ref}}(f)}=\frac{S_i(f)\cdot P_{ij}(f)\cdot G_j(f)}{S_i(f)\cdot P_{i,\mathrm{ref}}(f)\cdot G_{\mathrm{ref}}(f)}=\frac{G_j(f)}{G_{\mathrm{ref}}(f)} \tag{9}$$

Thus, 62WIX is chosen as a reference site and the spectral ratio was obtained by using Eq. (9) to acquire the site response of Station 62WUD, as shown in Fig. 10. Comparison with the observation shows (see Fig. 11) that the generalized inversion technique yields reliable results in this study.

4.2 Inversed site response

The site response of the selected 28 strong motion stations is calculated as expected by the separation of source, path and site effect. Figure 12 shows the inversion results compared with results from the HVSR method (Wen *et al*., 2011) and the 1-D theoretical computation. Note that due to the consideration of the free surface amplification, the site amplification obtained by the HVSR method is multiplied by a factor of 2. Note that good agreement exists between the results from the generalized inversion technique and HVSR method in some stations, such as 51CXQ, 51GYQ, 51GYS, 51QLY and 62WIX. For most of the stations, the site amplification obtained using the HVSR method is lower than that of the spectral inversion method, but they both yield identical predominant frequencies as observed in Fig. 12.

The site amplification by 1-D theoretical computation for all the stations except 51GYZ is much lower than the generalized inversion technique. The reason is that the available borehole data for each station only comes from 20 m's soil layer below the surface. The shear wave velocity beneath the depth of 20 m is around 400–600 m/s, even only 250 m/s at the Station 62WUD. Obviously these 20 m's soil layer can only induce a slight amplification relative to the bottom. Only the Station

Table 1 Parameters from earthquakes with similar hypocenter distance as Stations 62WIX and 62WUD

Earthquake ID EQ/yr/mo/da/hr/mn/sc	Magnitude M_s	Longitude (°)	Latitude (°)	Depth (km)	Hypocenter distance (km)	
					62WIX	62WUD
EQ080525162147	6.4	105.48	32.55	14	87.20	100.34
EQ080527163751	5.7	105.70	32.78	15	97.21	91.67
EQ080724035443	5.7	105.63	32.72	10	92.43	92.05
EQ080724150928	6.0	105.61	32.76	10	89.58	87.60
EQ080805174916	6.5	105.61	32.72	13	90.72	90.92

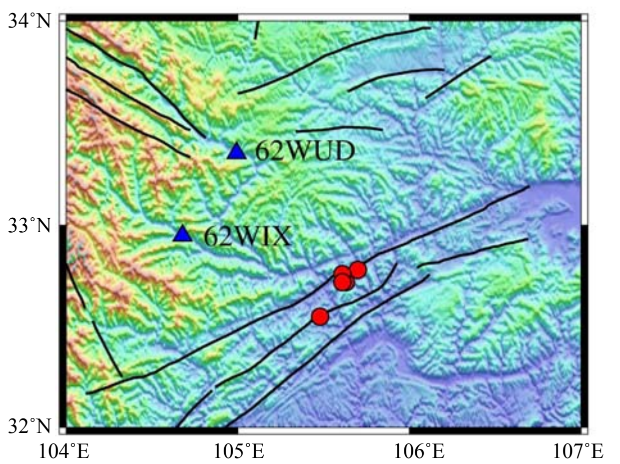

Fig. 9 Geographical location of Station 62WIX and 62WUD and the epicenter distribution of five earthquakes with the similar hypocenter distance of these two stations

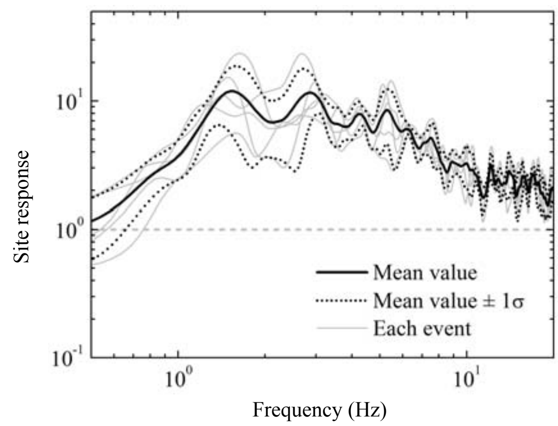

Fig. 10 Site response of Station 62WUD by using the SSR method based on the reference site 62WIX

51GYZ is distinctive where the site response by 1-D theoretical computation is in accordance with the one by the generalized inversion technique at the frequency range of 0.5–10 Hz as shown in Fig. 12. Beneath the

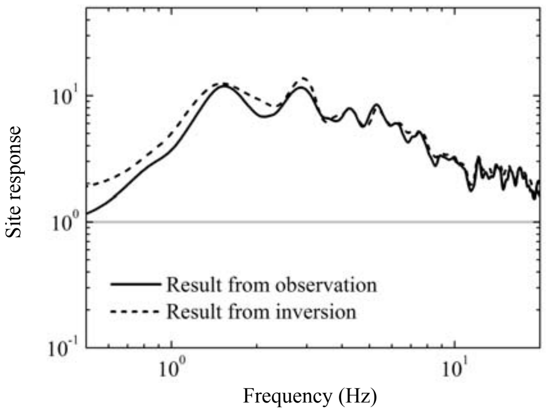

Fig. 11 Comparison of site response of Station 62WUD by using SSR method and GIT

20m-depth surface layer, a very hard rock of shear wave velocity of 1207 m/s exists as shown in Fig. 13.

4.3 Surface geology versus site response

As is well known, surface geology has a strong effect on the site response. For instance, in the present study, three Stations 51JZG, 51JZW and 51JZY with approximately identical surface geology, as shown in Table 2 and Fig. 14, are selected. Note that all these stations have nearly the same frequency-variation site amplification. Generally it has been recognized that for softer surface soil layers, the predominant frequency is lower and the site amplification is larger. From Fig. 14 (a), it is seen that the subsurface S-wave velocity of 51JZG is the smallest, 51JZW is medium and 51JZY is the largest, which means that the site of 51JZG is the softest, 51JZW is the second and 51JZY is the hardest. Their corresponding V_{s20s} are 260 m/s, 275 m/s and 369 m/s, respectively. A consistence result for the site amplification can be found from Fig. 14 (b), i.e., the 51JZG is the largest with the lowest predominant frequency, 51JZW is moderate and 51JZY is the smallest with the highest predominant frequency.

4.4 Predominant frequency and site amplification

Next, the predominant frequency and average site amplification are compared for different frequency bands calculated by the GIT and HVSR method (Wen *et al*., 2011). Appendix B gives the predominant frequency for each station by both methods. As Fig. 15 shows, the predominant frequency from both methods has a good agreement within 30% deviation. Furthermore, both the GIT and HVSR give close values of the calculated two predominant frequencies for Stations 51LXS and 51WUD. However, the average site amplification

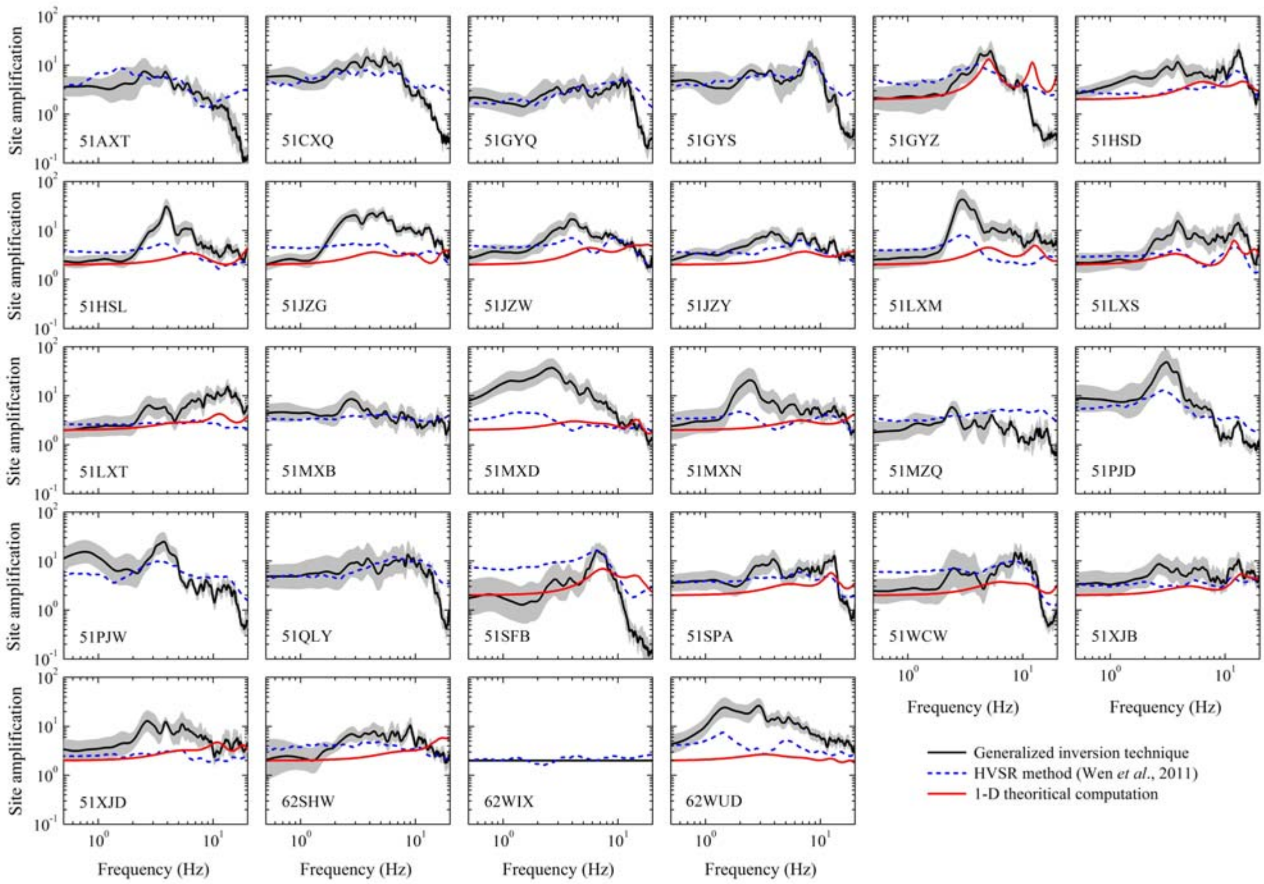

Fig. 12 Site responses at 28 strong motion stations calculated by generalized inversion technique, HVSR method and 1-D theoretical computation. Shaded area denotes the plus/minus one standard deviation range.

calculated by the HVSR method is lower than the generalized inversion technique for frequency bands 1.0–5.0 Hz, 5.0–10.0 Hz and 1.0–10.0 Hz as shown in Fig. 16. For the frequency 0.5–1.0 Hz band, there is only slight agreement between them. This is because the site response for this frequency band is slight, or even no amplification for some stations, as Fig.12 shows, almost equals to 2. Therefore, it can be concluded that the HVSR method can approximately evaluate the site predominant frequency but underestimates the site amplification. This conclusion has also been made by some other previous studies (Castro *et al*., 2004; Salazar *et al*., 2007; Hassani *et al*., 2011).

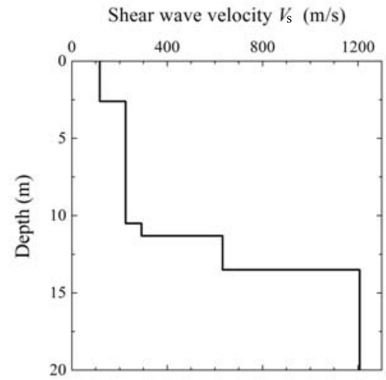

Fig. 13 Profile of subsurface S-wave velocity at the Station 51GYZ

Table 2 Surface geology information about the thickness and S-wave velocity V_s of different layers for Stations 51JZG, 51JZW and 51JZY

Surface geology	51JZG		51JZW		51JZY	
	Thickness (m)	V_s (m/s)	Thickness (m)	V_s (m/s)	Thickness (m)	V_s (m/s)
backfill	1.0	131	1.8	119	1.0	129
Silt with gravel	-	-	4.9	231	-	-
Slightly dense gravel	7.3	221	4.8	292	8.2	337
Medium dense gravel	11.7	324	5.5	397	7.0	458
Dense gravel	-	-	3.0	485	3.8	607

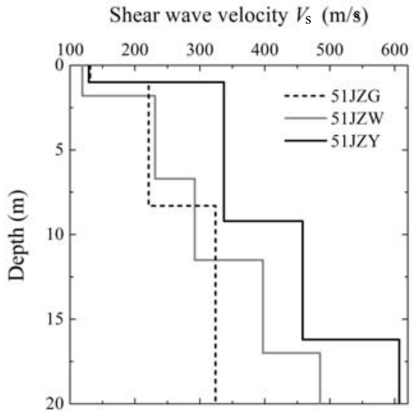

(a) Profile of subsurface S-wave velocity

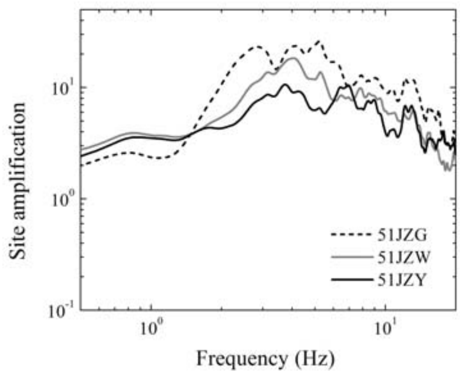

(b) Site amplification

Fig. 14 Demonstration of influences of the surface geology on the site response at different stations

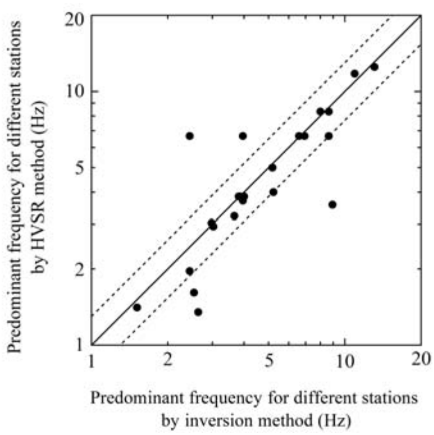

Fig. 15 Comparison of the predominant frequency calculated by generalized inversion technique and HVSR method. Dashed lines indicate 30% deviation

4.5 Relation between site amplification and V_{s20}

For some stations for which borehole data are available, average shear wave velocity of the upper 20m (V_{s20}) and the average site amplification for 0.5–1.0 Hz, 1.0–5.0 Hz, 5.0–10.0 Hz and 1.0–10.0 Hz frequency bands are calculated, as shown in Appendix B. A linear fitting in logarithmic scale is performed and the functions of site amplification as V_{s20} for each frequency band are obtained, as shown in Eqs. (10) to (13). The results show a weak correlation for the 0.5–1.0 Hz band, and a strong correlation for the other frequency bands as shown in Fig. 17. As mentioned in the previous section, for the 0.5–1.0 Hz frequency band, the site response is slight and most of the stations selected are located in high-mountain areas, where the shallow surface soil

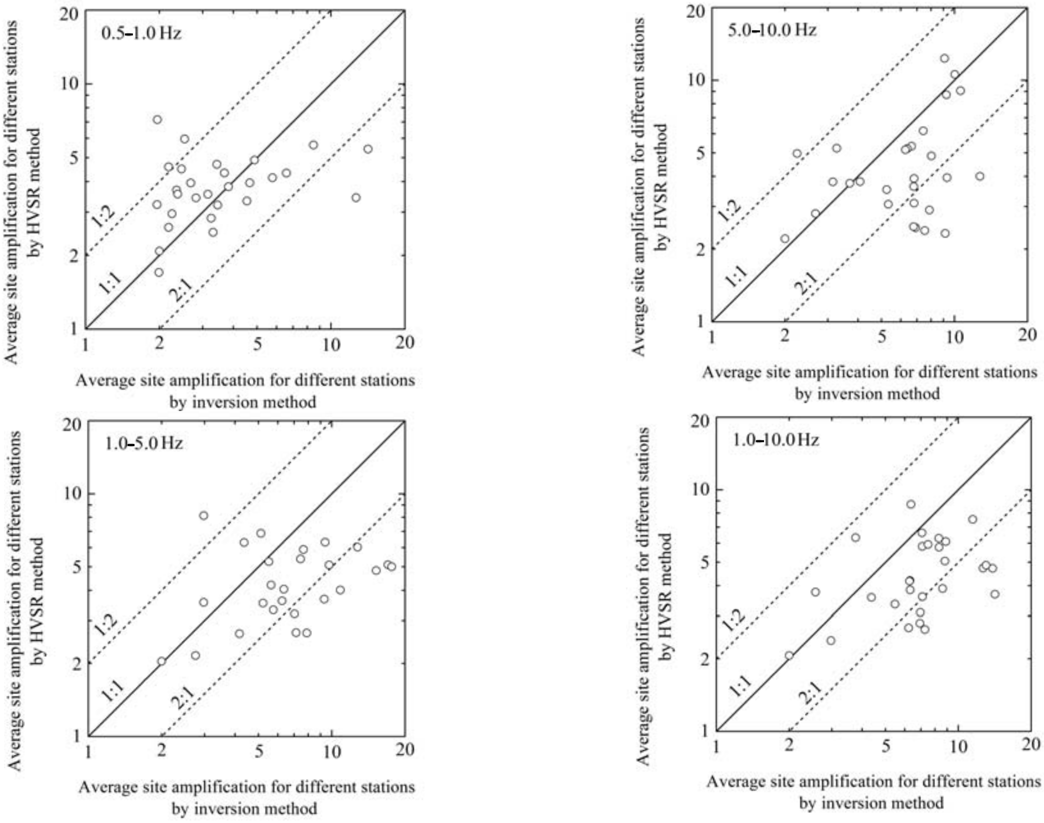

Fig. 16 Comparison of the average site amplification calculated by generalized inversion technique and HVSR method for 0.5–1.0 Hz, 1.0–5.0 Hz, 5.0–10.0 Hz and 1.0–10.0 Hz frequency bands. Dashed lines indicate 1:2 and 2:1 correspondence

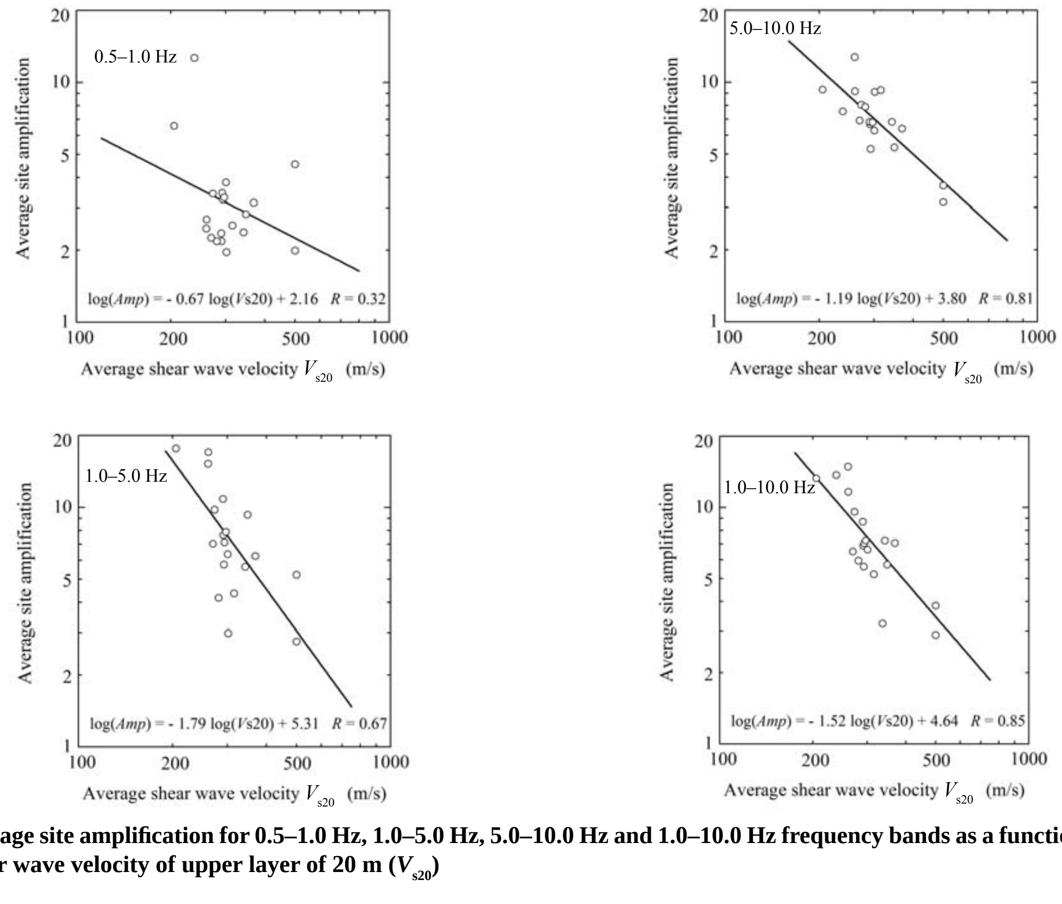

Fig. 17 Average site amplification for 0.5–1.0 Hz, 1.0–5.0 Hz, 5.0–10.0 Hz and 1.0–10.0 Hz frequency bands as a function of average shear wave velocity of upper layer of 20 m (V_{s20})

layers only induce high-frequency amplification.

$$\log(\mathrm{Amp}_{(0.5\text{-}1.0\mathrm{Hz})}) = -(0.67 \pm 0.47) \cdot \log(V_{s20}) + (2.16 \pm 1.16) \quad (R = 0.32) \tag{10}$$

$$\log(\mathrm{Amp}_{(1.0\text{-}5.0\mathrm{Hz})}) = -(1.79 \pm 0.47) \cdot \log(V_{s20}) + (5.31 \pm 1.16) \quad (R = 0.67) \tag{11}$$

$$\log(\mathrm{Amp}_{(5.0\text{-}10.0\mathrm{Hz})}) = -(1.19 \pm 0.21) \cdot \log(V_{s20}) + (3.80 \pm 0.52) \quad (R = 0.81) \tag{12}$$

$$\log(\mathrm{Amp}_{(1.0\text{-}10.0\mathrm{Hz})}) = -(1.52 \pm 0.23) \cdot \log(V_{s20}) + (4.64 \pm 0.57) \quad (R = 0.85) \tag{13}$$

Note that even though Eqs. (11), (12) and (13) show strong correlation (large R value) between the average site amplification and the V_{s20}, care must be taken when used in engineering applications because the nonlinear behavior of soil under strong ground motion shaking has not yet been considered.

4.6 Soil nonlinearity identification for aftershocks

To study the soil nonlinearity effect, the site amplifications under strong and weak motions are discussed and compared in this section. Under weak motion, the results for site amplification by using the generalized inversion technique for all sites selected have been obtained (see Fig.12). For strong motion, corresponding results can be obtained by using a transform of Eq. (3) as follows:

$$G_j^{\,s}(f) = \frac{O_{ij}^{\,s}(f) \cdot R_{ij}^{\,s}}{S_i(f) \cdot \exp(-\pi f R_{ij}^{\,s} / Q(f) \cdot V_s)} \tag{14}$$

Here, to distinguish the strong motion from the weak one, a superscript s is introduced for $G_j(f)$, $O_{ij}(f)$ and R_{ij}. The path effect in terms of the frequency-dependent quality factor $Q(f)$, and the source spectrum $S_i(f)$ has been solved by the above generalized inversion.

As described in Subsection 3.1, the weak motion in this study is defined as the average PGA of two horizontal components and is below 100 cm/s^2. Thus, sixteen recordings with an average PGA above 100 cm/s^2 are selected to analyze the strong motion effect in the Wenchuan aftershocks. The parameters of the recordings are summarized in Table 3.

Comparison between the site amplifications of the weak and strong motions (see Fig. 18) indicates that the soil nonlinearity is identified only in the ground motions at station 51SFB in the Earthquakes EQ080512144315 and EQ080512150134 corresponding to No.3 and No.4 in Table 3. The site amplification obviously shifts towards the lower frequency under strong motion than the weak motion, namely lower predominant frequency and deamplification in the high frequency part. Their average PGA is 135.1 cm/s^2 and 105.7 cm/s^2, respectively. This leads to a preliminary conclusion that Site 51SFB responds to the soil nonlinearity response when the PGA of its ground motion exceeds 100 cm/s^2 during the aftershocks of Wenchuan earthquake.

An interesting phenomenon observed from Fig.18 is that for site 51WCW, the site amplification under Earthquake EQ080512151345 seems much larger than the weak motion. This can also be noticed for this site under Earthquake EQ080512182339, and for Site 51MZQ under Earthquake EQ080512162140 and EQ080512174224, corresponding to No.5, No.7, No.8, and No.9 of Table 3, respectively. In fact, such extremely large amplification is not mainly contributed from the site effect, instead it is most likely from the seismic

Table 3 Recordings identified as strong motion for analyzing soil nonlinearity in the aftershocks of Wenchuan earthquake

No.	Earthquake ID EQ/yr/mo/da/hr/mn/sc	Station ID	Magnitude M_s	Hypocenter distance (km)	PGA (cm/s^2)		
					EW	NS	Mean
1	EQ080512144315	51LXM	6.3	45.46	129.8	128.9	129.4
2	EQ080512144315	51LXT	6.3	40.65	108.2	105.0	106.6
3	**EQ080512144315**	**51SFB**	**6.3**	**20.72**	**144.7**	**125.6**	**135.1**
4	**EQ080512150134**	**51SFB**	**5.5**	**46.34**	**92.2**	**119.2**	**105.7**
5	EQ080512151345	51WCW	4.7	20.37	238.4	199.5	219.0
6	EQ080512162140	51MXB	5.5	26.23	84.1	161.4	122.7
7	EQ080512162140	51MZQ	5.5	20.28	117.5	103.1	110.3
8	EQ080512174224	51MZQ	5.3	20.28	163.1	296.6	229.9
9	EQ080512182339	51WCW	5.0	21.86	141.9	148.0	145.0
10	EQ080512191101	51LXM	6.3	48.09	216.0	188.0	202.0
11	EQ080512191101	51LXT	6.3	41.09	208.4	193.2	200.8
12	EQ080512191101	51MXN	6.3	41.97	103.1	101.9	102.5
13	EQ080513075446	51LXT	5.2	27.10	164.7	113.6	139.2
14	EQ080516132547	51LXM	5.9	34.10	142.0	138.0	140.0
15	EQ080516132547	51LXS	5.9	37.59	156.0	136.8	146.4
16	EQ080525162147	51GYQ	6.4	52.46	161.9	127.2	144.6

Note: the boldface means the soil nonlinearity is found evidently

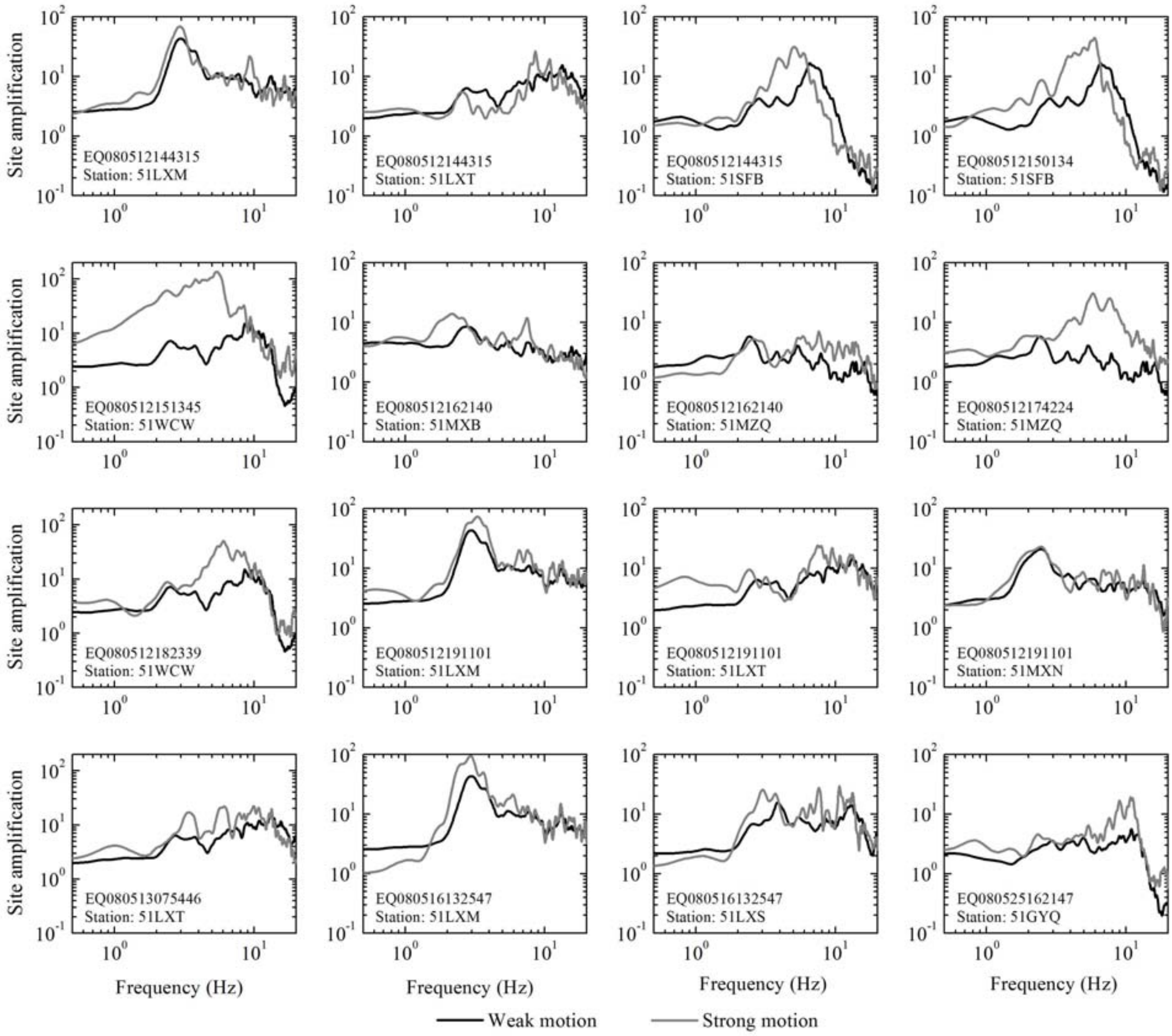

Fig. 18 Comparison of site amplification calculated by weak motion and strong motion in the aftershocks of Wenchuan earthquake

source. The common feature of these four recordings is that their hypocenter distances are nearly around 20 km (see Table 3), thus they actually belong to the near-field ground motions. Sometimes the near-field ground motion have the typical characteristics of impulsive nature caused by the propagation of fault rupture such as polarization and directivity (Somerville *et al*., 1997), or the uppermost depth of the fault and the location of the asperity (Inoue and Miyatake, 1998). The acceleration time-histories of these four unusual recordings plotted in Fig. 19 illustrate that the No.5 and No.8 recordings have a quite obvious impulsive feature which is perhaps caused by the possible reasons stated above, which induces a large difference in the site amplification as shown in Fig. 18. Meanwhile, after checking the No.3 and No. 4 recordings for the soil nonlinearity that has been identified, the same source effect as described above is found. Because it can be seen from Fig. 18 that their site amplification under strong motion is a little bit larger than that under weak motion. Their time-histories are also plotted in Fig. 18 and the impulsive amplitude is found as well.

4.7 Soil nonlinearity identification for main shock

As Li *et al*. (2008) presented, many large strong motion recordings were accumulated in the main shock of Wenchuan earthquake, such as those recorded at Station 51MZQ with a PGA of -824.6 cm/s^2, Station 51WCW with a PGA of 957.3 cm/s^2, Station 51SFB with a PGA of -585.7 cm/s^2, etc. It is necessary to discuss whether these recordings are affected by the soil nonlinearity. Among the 28 stations of the dataset used herein, only 51GYQ did not capture the recording in the main shock because of the instrument malfunction. Thus, another 27 recordings are added into the dataset to take the generalized inversion again based on an assumption that these recordings were obtained from another 26 different stations except the reference Station 62WIX. In other words, the matrix $\boldsymbol{A}$, vector $\boldsymbol{x}$ and $\boldsymbol{b}$ of Eq. (5) would be enlarged as follows:

$$\begin{bmatrix} \boldsymbol{A} & \boldsymbol{0} \\ \boldsymbol{0} & \boldsymbol{A}' \end{bmatrix} \cdot \begin{bmatrix} \boldsymbol{x} \\ \boldsymbol{x}' \end{bmatrix} = \begin{bmatrix} \boldsymbol{b} \\ \boldsymbol{b}' \end{bmatrix} \tag{15}$$

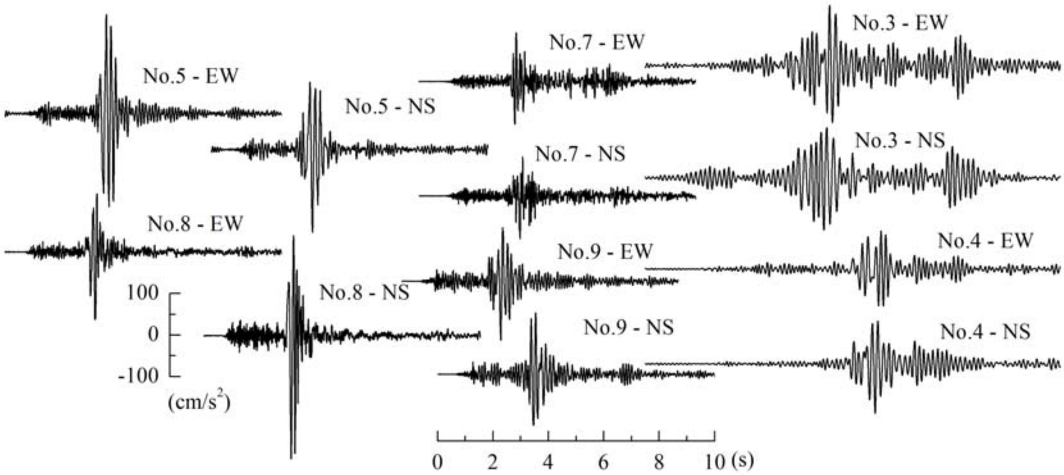

Fig. 19 Time-histories of four recordings with unusually large site amplification and time-histories of 51SFB recordings identified the occurrence of the soil nonlinear response

where $\boldsymbol{A}'$ denotes the diagonal unit matrix. Vector $\boldsymbol{x}'$ represents the additional 26 unknown variables that are the unsolved site response under the main shock. Vector $\boldsymbol{b}'$ denotes the term on the left side of Eq. (4) calculated by the recordings from the main shock. Note that the matrix $\boldsymbol{A}$, vector $\boldsymbol{x}$ and $\boldsymbol{b}$ in Eq. (15) are slightly different from those in Eq. (5) due to the added data from the main shock for reference Station 62WIX.

By solving Eq. (15), the site responses of the 26 stations under both the main shock (namely strong motion) and under the aftershocks (namely weak motion) can be obtained and compared. As a result, the soil nonlinearity under the main shock can be identified.

However, Eq. (15) is established upon the basic assumption of a point source earthquake. In fact, for the great Wenchuan earthquake, the fault rupture process took a long time and spanned a great distance. The point source assumption is not suitable for such a large earthquake and the influence of the distance R_{ij} should be considered (Field *et al*., 1997 and 1998).

In this study, a new source-to-site distance measurement called asperity distance D_{Aspt} defined in Eq. (16) is proposed.

$$\ln D_{\mathrm{Aspt}} = \frac{1}{A}\int_{\Sigma} \ln D(x,\ \xi)\ \mathrm{d}s \tag{16}$$

where $D(x, \xi)$ denotes the distance from station x to a point ξ on the asperity region Σ, and A is the total area of the asperity. D_{Aspt} represents a mean distance from the station to asperity. For the slip model of the Wenchuan earthquake, the inversion result of the finite fault model from USGS is used. According to the definition of asperity area by Somerville *et al*. (1999), two asperities for the Wenchuan earthquake are identified as shown in Fig. 20, and the D_{Aspt} is calculated by Eq. (16). Meanwhile, another three types of source-to-site distance measurements that have been widely used for ground motion attenuation analysis are also calculated. The three kinds of source-to-site distance measurements include: the rupture distance (D_{Rup}, the shortest distance between the station and the rupture surface), the Joyner–Boore distance (D_{JB}, the closest horizontal distance from the station to the vertical projection of the rupture onto Earth's surface) and the hypocentral distance D_{Hyp}. All of the calculated results based on the above four types of distance measurements for all stations are given in Appendix C.

Figure 21 shows the inversion results of site amplification for each station under weak motion and strong motion by means of the different distance measurements. If the low frequency part (0.5–1.0 Hz) is considered, the site amplification should be close to 2 not only under the weak motion but also under the strong motion since there is no considerable amplification in this frequency band as explained above. However, the site amplification for most of the stations under strong motion characterized by D_{Hyp} is much lower than 2 as seen in Fig. 21, which means that the D_{Hyp} is unreasonable for the main shock to characterize the source-to-site distance.

The reference Station 62WIX is located at the opposite direction from the strike of the fault, which is much closer to two asperities than to the hypocenter

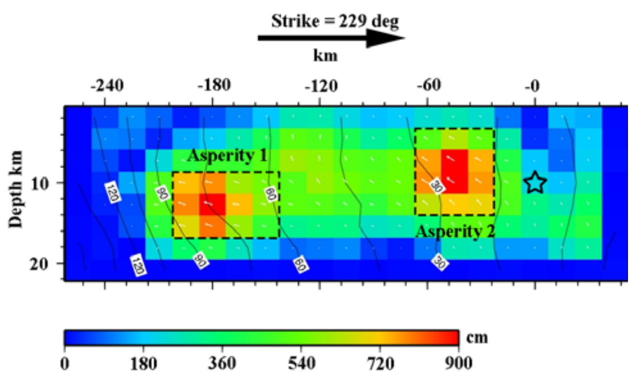

Fig. 20 Two identified asperities for Wenchuan earthquake. Fault slip model is derived from USGS. The asterisk represents the epicenter

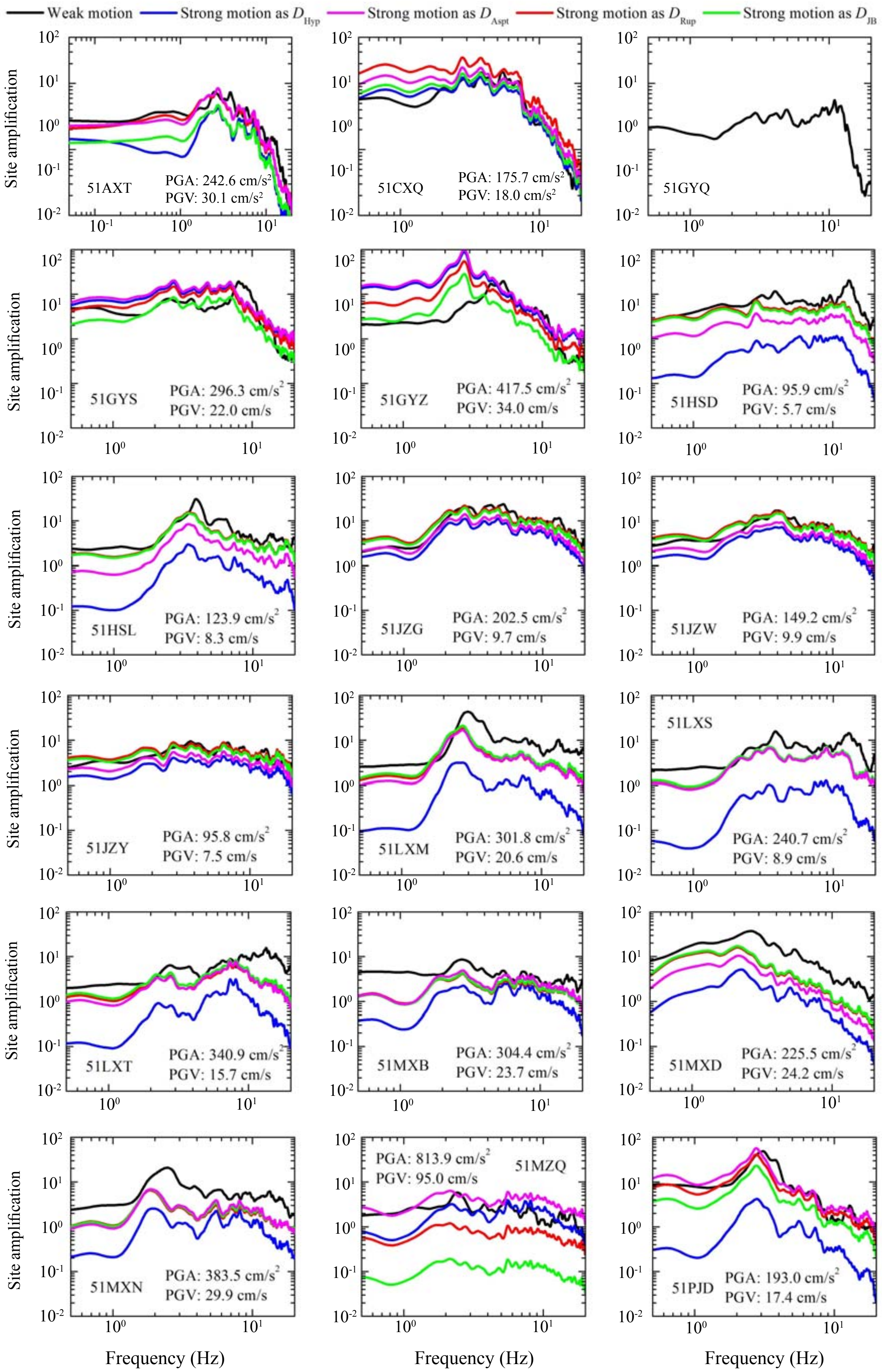

Fig. 21 Comparison of site amplification under weak motion of the aftershocks and strong motion of the main shock in Wenchuan earthquake. Four kinds of distance measurements are used to characterize the source-to-site distance in the main shock

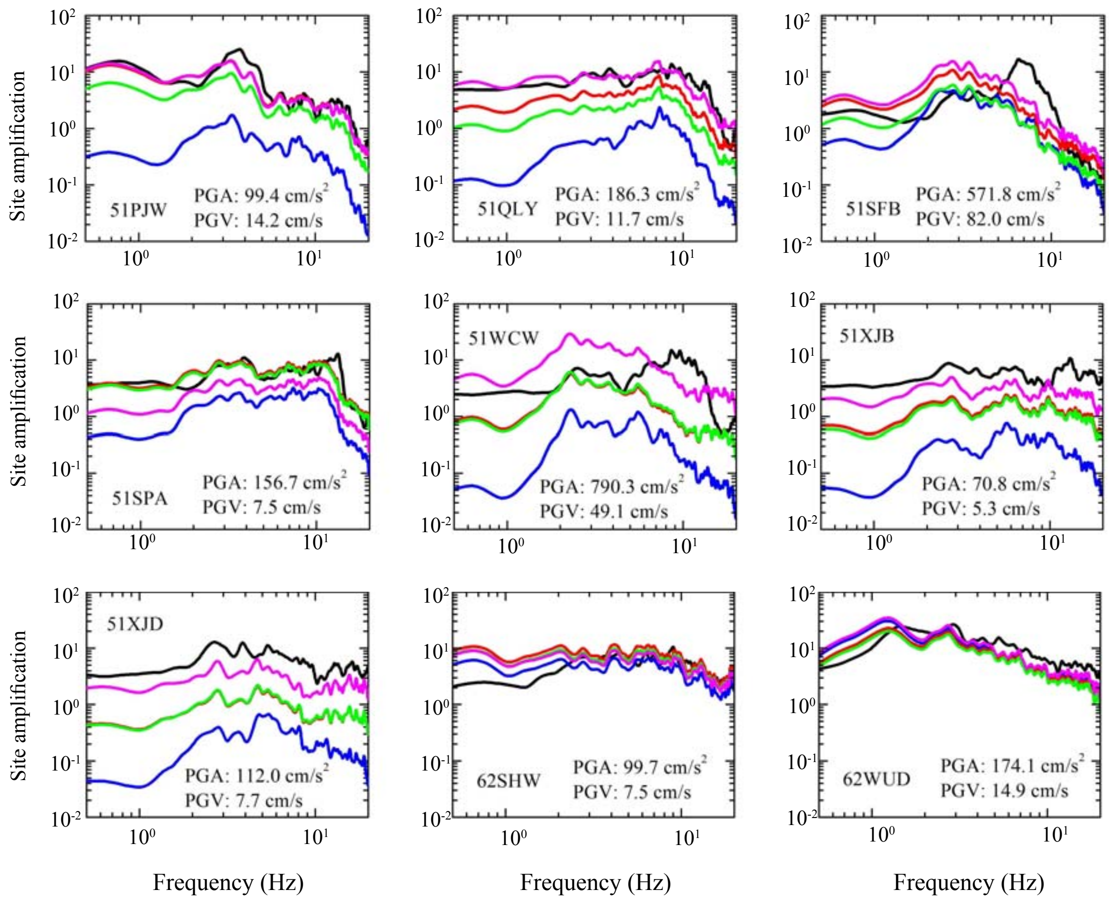

Fig. 21 Continued

that can be observed in Fig. 20. Therefore, the D_{Hyp} overestimates the source-to-site distance for this station, which will lead to an overestimation of the source spectrum of the main shock according to Eq. (3). As a result, for most of the other stations, the site response will be underestimated spontaneously according to Eq. (1). In Fig. 21, it can be seen that a good improvement has been made by using the new definition of D_{Aspt}. In addition, the comparison shows that there are no large differences between the D_{Rup} and D_{JB}, in particular for moderate and far field stations.

Figure 21 also displays an apparent evidence of the soil nonlinearity for Stations 51GYZ, 51SFB, and 51WCW with a significant shift of the predominant frequency F_{p} to the lower frequency range. Note that the recordings from these three stations have high PGA and PGV. The soil nonlinearity can also be identified for Stations 51GYS, 51LXT, 51MXD, 51MXN, and 62WUD, which have the same feature of the F_{p} shifting.

It is possible to find the correlation between the nonlinearity level and ground motion level corresponding to the PGA and PGV. First, a baseline correction for the main shock recordings is performed by using the method proposed by Boore (2001), the corrected PGAs and PGVs are extracted and shown in Appendix C. Then, the ratios of the F_{p} at each station under weak motion and strong motion can be calculated, and the results are provided in Appendix C. The ratios of the F_{p} versus the mean PGA and PGV of the two horizontal components are shown in Fig. 22. Note that when the PGA > 300 cm/s^2 or PGV > 20 cm/s, the F_{p} for strong motion becomes much less than the weak motion, revealing that the soil exhibits very strong nonlinearity. Looking at the shaded area of Fig. 22, it can be seen that the nonlinearity level becomes larger as the PGA value increases. Note that for Station 51MZQ, even for PGAs larger than 800 cm/s^2 and PGVs near to 100 cm/s, there is no exact evidence to show the soil nonlinearity in Fig. 21 and Fig. 22. From the surface geology of Station 51MZQ, only a 1.5m-thick overburden above the soft bedrock (shear velocity nearly 400 m/s) can be found, which shows the unlikelihood of soil nonlinearity.

In addition, the site condition (V_{s20}) of the station is checked to determine if it has an effect on soil nonlinearity. Figure 22 plots the F_{p} versus V_{s20} as well. Even though the hard soil Stations 51WCW, 51SFB, 51GYZ and 51LXT have a higher level of nonlinearity than the soft soil Stations 62WUD and 51MXD, their ground motion levels (PGA or PGV) are also higher. Thus, for this case, if the effect of the ground motion level cannot be removed, the effect of the site conditions on the soil nolinearity cannot be evaluated.

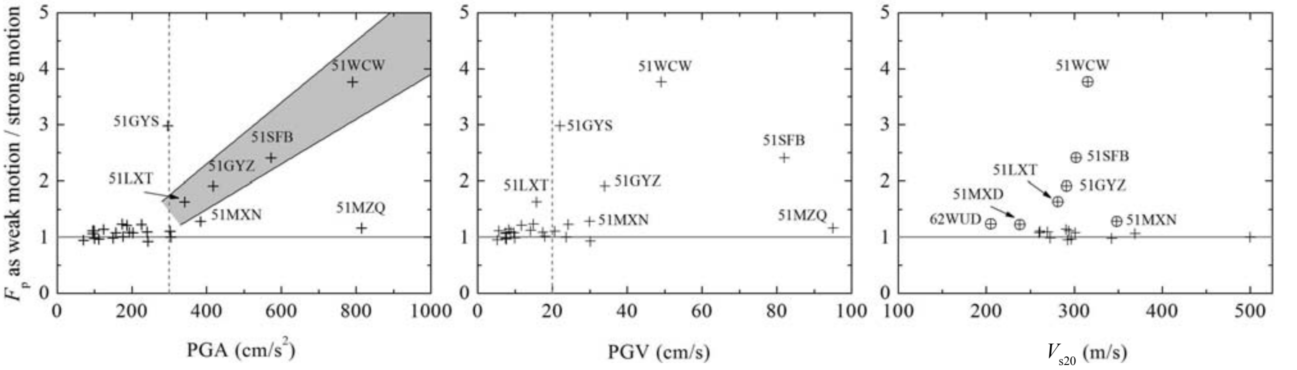

Fig. 22 The predominant frequency F_p as weak motion over strong motion versus PGA, PGV and V_{s20}, respectively. Dashed lines indicate the threshold value of the PGA and PGV when the soil behaves nonlinearly. Shaded area shows the level of nonlinearity varies with PGA. The circle within a cross means the station that has apparent evidence of the soil nonlinearity

5 Conclusions

A large number of strong motion recordings obtained in the main shock and aftershocks of the 2008 Great Wenchuan earthquake were used in this study. Using the generalized inversion technique, the source, path and site effect of these recordings were separated and the inversed site effects were analyzed. The following conclusions can be drawn:

(1) The site response at 28 strong motion stations was evaluated by using the generalized inversion technique, Horizontal-to-Vertical Spectral Ratio (HVSR) method and 1-D theoretical computation. The comparison shows the 1-D theoretical computation underestimated the results for most of stations. This could be because only the uppermost 20 m-thick borehole data are available for these strong motion stations. The comparison also shows that the HVSR method can reasonably estimate the site predominant frequency but will underestimate the site amplification.

(2) The site response for three stations, 51JZG, 51JZW and 51JZY, with similar surface geology shows the site amplification obviously depends on the thickness and shear wave velocity of the soil layer.

(3) The functions of the site amplification related to V_{s20} (the average uppermost-20 m shear wave velocity) for 1.0–5.0 Hz, 5.0–10.0 Hz and 1.0–10.0 Hz frequency bands were given, respectively, in the Wenchuan area.

(4) A new distance measurement called the asperity distance D_{Aspt} was proposed to reasonably characterize the source-to-site distance for large earthquakes such as the Wenchuan earthquake, and was verified to be much better than other kinds of distance measurements, including the rupture distance (D_{Rup}), Joyner–Boore distance (D_{JB}) and hypocentral distance (D_{Hyp}).

(5) The strong motion recordings of the main shock of the Wenchuan earthquake were added into the initial dataset, and the generalized inversion was implemented again. The comparison of site response under the main shock and aftershocks shows that soil nonlinearity occurred in the main shock at ten stations among the selected 28 stations. It was found that a threshold of PGA > 300 cm/s^2 or PGV > 20 cm/s obviously existed for the soil nonlinearity in the Wenchuan earthquake and the nonlinearity level significantly depended on the PGA or PGV level. The soil nonlinearity in the aftershocks was also identified and only the soil at the station coded 51SFB had evidence of the nonlinearity.

(6) The above results show that the Generalized Inversion Technique (GIT) can be used to reasonably and effectively evaluate the site effect. There is no doubt that the engineering investigation (e.g., drilling, wave velocity test, etc.) method offers the advantages of simplicity and practicality. However, conversely, its accuracy and scientificity continue to be a controversial issue with respect to the shallow exploration depth used to represent the site effect of limited soil layers, especially the V_{s20} proposed in the Chinese code classification of the site condition by using only a 20 m surface soil layer. The GIT can explore the real site response of deep soil by using the actual observed recordings; therefore, its application in engineering practice is recommended.

Acknowledgement

The authors appreciate the two anonymous reviewers who provided the valuable comments and suggestions that significantly improve this article. This study was conducted as a part of the training course of International Institute of Seismology and Earthquake Engineering, Building Research Institute, Japan that is financially supported by Japan International Cooperation Agency from Oct., 2011 to Sep., 2012. Appreciation will be given to Dr. Yadab. P. Dhakal, Ph.D candidates Rhommel Grutas and Zaineh, Hussam Eldein from Yamanaka Laboratory of Tokyo Institute of Technology for their kind discussions and helpful proposals in data processing and generalized inversion in this study. Thanks will also be given to the editor of this Journal Prof. Xiong Jianguo for his kind proofreading that makes a good improvement for this article. We also thank the China National Strong Motion Network Center for

sharing the Wenchuan earthquake strong motion data.

References

Andrews DJ (1986), "Objective Determination of Source Parameters and Similarity of Earthquakes of Different Size," *Geophysical Monographs Series*, **37**: 259–267.

Beresnev IA, Atkinson GM, Johnson PA and Field EH (1998), "Stochastic Finite-fault Modeling of Ground Motions from the 1994 Northridge, California, Earthquake. II. Widespread Nonlinear Response at Soil Sites," *Bulletin of the Seismological Society of America*, **88**(6): 1402–1410.

Beresnev IA and Wen KL (1996), "Nonlinear Soil Response—a Reality," *Bulletin of the Seismological Society of America*, **86**(6): 1964–1978.

Bo JS, Qi WH, Liu HS, Liu B, Liu DD and Sun YW (2009), "Abnormality of Seismic Intensity in Hanyuan during Wenchuan Earthquake," *Journal of Earthquake Engineering and Engineering Vibration*, **29**(6): 53–63. (in Chinese)

Boatwright J, Fletcher JB and Fumal TE (1991), "A General Inversion Scheme for Source, Site, and Propagation Characteristics Using Multiply Recorded Sets of Moderate-sized Earthquakes," *Bulletin of the Seismological Society of America*, **81**(5): 1754–1782.

Boore DM (2001), "Effect of Baseline Corrections on Displacements and Response Spectra for Several Recordings of the 1999 Chi-Chi, Taiwan," *Bulletin of the Seismological Society of America*, **91**(5): 1199–1211.

Boore DM and Joyner WB (1997), "Site Amplifications for Generic Rock Sites," *Bulletin of the Seismological Society of America*, **87**(2): 327–341.

Borcherdt RD (1970), "Effects of Local Geology on Ground Motion Near San Francisco Bay," *Bulletin of the Seismological Society of America*, **60**(1): 29–61.

Brune JN (1970), "Tectonic Stress and the Spectra of Seismic Shear Waves from Earthquakes," *Journal of Geophysical Research*, **75**(26): 4997–5009.

Brune JN (1971), "Correction (to Brune, 1970)," *Journal of Geophysical Research*, **76**(20): 5002.

Castro RR, Pacor F, Bindi D, Franceschina G and Luzi L (2004), "Site Response of Strong Motion Stations in the Umbria, Central Italy, Region," *Bulletin of the Seismological Society of America*, **94**(2): 576–590.

Drouet S, Chevrot S, Cotton F and Souriau A (2008), "Simultaneous Inversion of Source Spectra, Attenuation Parameters, and Site Responses: Application to the Data of the French Accelerometric Network," *Bulletin of the Seismological Society of America*, **98**(1): 198–219.

Dutta U, Biswas N, Martirosyan A, Papageorgiou A and Kinoshita S (2003), "Estimation of Earthquake Source Parameters and Site Response in Anchorage, Alaska from Strong-motion Network Data Using Generalized Inversion Method," *Physics of the Earth and Planetary Interiors*, **137**(1-4): 13–29.

Dutta U, Martirosyan A, Biswas N, Papageorgiou A and Combellick R (2001), "Estimation of S-wave Site Response in Anchorage, Alaska, from Weak-motion Data Using Generalized Inversion Method," *Bulletin of the Seismological Society of America*, **91**(2): 335–346.

Field EH and Jacob KH (1995), "A Comparison and Test of Various Site-response Estimation Techniques, Including Three That Are Not Reference-site Dependent," *Bulletin of the Seismological Society of America*, **85**(4): 1127–1143.

Field EH, Johnson PA, Beresnev IA and Zeng YH (1997), "Nonlinear Ground-motion Amplification by Sediments during the 1994 Northridge Earthquake," *Nature*, **390**: 599–602.

Field EH, Zeng YH, Johnson PA and Beresnev IA (1998), "Nonlinear Sediment Response during the 1994 Northridge Earthquake: Observations and Finite Source Simulations," *Journal of Geophysical Research*, **103**(B11): 26869–26883.

Fletcher JB and Boatwright J (1991), "Source Parameters of Loma Prieta Aftershocks and Wave Propagation Characteristics along the San Francisco Peninsula from a Joint Inversion of Digital Seismograms," *Bulletin of the Seismological Society of America*, **81**(5): 1783–1812.

Francisco JCG, Rodriguez M, Field EH and Hatzfeld D (1997), "Topographic Site Effects. A Comparison of Two Nonreference Methods," *Bulletin of the Seismological Society of America*, **87**(6): 1667–1673.

Harmsen SC (1997), "Bulletin of Determination of Site Amplification in the Los Angeles Urban Area from Inversion of Strong-motion Records," *Bulletin of the Seismological Society of America*, **87**(4): 866–887.

Hartzell S (1992), "Site Response Estimation from Earthquake Data," *Bulletin of the Seismological Society of America*, **82**(6): 2308–2327.

Hartzell S (1998), "Variability in Nonlinear Sediment Response during the 1994 Northridge, California, Earthquake," *Bulletin of the Seismological Society of America*, **88**(6): 1426–1437.

Hasemi A, Matsuzawa T, Hasegawa A, Umino N, Kono T, Hori S, Ito A, Suzuki S and Ishikawa H (1997), "Q and Site Amplification Factors of Hard-rock Region in the Kitakami Massif, Northeastern Japan," *Journal of Physics of the Earth*, **45**(6): 417–431.

Hassani HZ, Farjoodi J and Ansari A (2011), "Estimation of Site Amplification, Attenuation and Source Spectra of S-waves in the East-Central Iran," *Soil Dynamics and Earthquake Engineering*, **31**(10): 1397–1413.

Hoshiba M (2003), "Fluctuation of Wave Amplitude Even When Assuming Convolution of Source, Path and Site Factors—Effect of Rupture Directivity," *Physics of the Earth and Planetary Interiors*, **137**(1-4): 45–65.

Husid P (1967), "Gravity Effects on the Earthquake Response of Yielding Structures," *PhD. thesis*, California Institute of Technology, 1–153.

Inoue T and Miyatake T (1998), "3D Simulation of Near-field Strong Ground Motion Based on Dynamic

Modeling," *Bulletin of the Seismological Society of America*, **88**(6): 1445–1456.

Iwata T and Irikura K (1986), "Separation of Source, Propagation and Site Effects from Observed S-wave," *Zisin* (*Journal of the Seismological Society of Japan*), **39**: 579–593. (in Japanese with English Abstract)

Iwata T and Irikura K (1988), "Source Parameters of the 1983 Earthquake Sequence," *Journal of Physics of the Earth*, **36**(4): 155–184.

Kato K, Takemura M, Ikeura T, Urao K, and Uetake T (1992), "Preliminary Analysis for Evaluation of Local Site Effect from Strong Motion Spectra by an Inversion Method," *Journal of Physics of the Earth*, **40**(1): 175–191.

Lawson CL and Hanson RJ (1974), *Solving Least Squares Problem*, New Jersey: Prentice-Hall, Inc., Englewood Cliffs, 1–337.

Li XJ (2009), Uncorrected Acceleration Records from Fixed Observation for Wenchuan Ms8.0 Aftershocks, Beijing: Seismological Publishing House, 1–600. (in Chinese)

Li XJ, Zhou ZH, Yu HY, Wen RZ, Lu DW, Huang M, Zhou YN and Cu JW (2008), "Strong Motion Observations and Recordings from The Great Wenchuan Earthquake," *Earthquake Engineering and Engineering Vibration*, **7**(3): 235–246.

Matsunami K, Zhang WB, Irikura K and Xie LL (2003), "Estimation of Seismic Site Response in the Tangshan Area, China, Using Deep Underground Records," *Bulletin of the Seismological Society of America*, **93**(3): 1065–1078.

McCann MWJ and Shah HC (1979), "Determining Strong Motion Duration of Earthquakes," *Bulletin of the Seismological Society of America*, **69**(4): 1253–1265.

Moya A, Aguirre J and Irikura K (2000), "Inversion of Source Parameters and Site Effects from Strong Ground Motion Records Using Genetic Algorithms," *Bulletin of the Seismological Society of America*, **90**(4): 977–992.

Moya A and Irikura K (2003), "Estimation of Site Effects and Q Factor Using a Reference Event," *Bulletin of the Seismological Society of America*, **93**(4): 1730–1745.

Parolai S, Bindi D, Baumbach M, Grosser H, Mikereit C, Karakisa S and Zunbul S (2004), "Comparison of Different Site Response Estimation Techniques Using Aftershocks of the 1999 Izmit Earthquake," *Bulletin of the Seismological Society of America*, **94**(3): 1096–1108.

Roumelioti Z and Beresnev IA (2003), "Stochastic Finite-fault Modeling of Ground Motions from the 1999 Chi-Chi, Taiwan, Earthquake: Application to Rock and Soil Sites with Implications for Nonlinear Site Response," *Bulletin of the Seismological Society of America*, **93**(4): 1691–1702.

Salazar W, Sardina V and Cortina JDA (2007), "Hybrid Inversion Technique for the Evaluation of Source, Path, and Site Effects Employing S-wave Spectra for Subduction and Upper-crustal Earthquakes in El Salvador," *Bulletin of the Seismological Society of America*, **97**(1B): 208–221.

Seed HB, Romo MP, Sun JI, Jaime A and Lysmer J (1988), "The Mexico Earthquake of September 19, 1985-Relationships between Soil Conditions and Earthquake Ground Motions," *Earthquake Spectra*, **4**(4): 687–729.

Shoji Y and Kamiyama M (2002), "Estimation of Local Site Effects by a Generalized Inversion Scheme Using Observed Records of 'Small-Titan'," *Soil Dynamics and Earthquake Engineering*, **22**(9-12): 855–864.

Somerville PG, Irikura K, Graves RW, Wald D, Abrahamson NA, Iwasaki Y, Kagawa T, Smith N and Kowada A (1999), "Characterizing Crustal Earthquake Slip Models for the Prediction of Strong Ground Motion," *Seismological Research Letters*, **70**(1): 59–80.

Steidl JH, Tumarkin AG and Archuleta RJ (1996), "What is a Reference Site?" *Bulletin of the Seismological Society of America*, **86**(6): 1733–1748.

Somerville PG, Smith NF, Graves RW and Abrahamson NA (1997), "Modification of Empirical Strong Ground Motion Attenuation Relations to Include the Amplitude and Duration Effects of Rupture Directivity," *Seismological Research Letters*, **68**(1): 199–222.

Su F, Anderson JG. and Zeng YH (1998), "Study of Weak and Strong Ground Motion Including Nonlinearity from the Northridge, California, Earthquake Sequence," *Bulletin of the Seismological Society of America*, **88**(6): 1411–1425.

Takemura M, Kato K, Ikeura T and Shima E (1991), "Site Amplification of S-waves from Strong Motion Records in Special Relation to Surface Geology," *Journal of Physics of the Earth*, **39**(3): 537–552.

Tsuda K, Koketsu K, Hisada Y and Hayakawa T (2010), "Inversion Analysis of Site Responses in the Kanto Basin Using Data from a Dense Strong Motion Seismograph Array," *Bulletin of the Seismological Society of America*, **100**(3): 1276–1287.

Wang D and Xie LL (2010), "Study on Response Spectral Acceleration from the Great Wenchuan, China Earthquake of May 12, 2008," *Journal of Earthquake Engineering*, **14**(6): 934–952.

Wen RZ, Ren YF and Shi DC (2011), "Improved HVSR Site Classification Method for Free-field Strong Motion Stations Validated with Wenchuan Aftershock Recordings," *Earthquake Engineering and Engineering Vibration*, **10**(3): 325–337.

Wen RZ, Ren YF, Zhou ZH and Shi DC (2010a), "Preliminary Site Classification of Free-field Strong Motion Stations Based on Wenchuan Earthquake Records," *Earthquake Science*, **23**(1):101–110.

Wen ZP, Xie JJ, Gao MT, Hu YX and Chau KT (2010b), "Near-source Strong Ground Motion Characteristics of the 2008 Wenchuan Earthquake," *Bulletin of the Seismological Society of America*, **100**(5B): 2425–2439.

Yamanaka H, Nakamura A, Kurita K and Seo K (1998), "Evaluation of Site Effects by an Inversion of S-wave Spectra with a Constraint Condition Considering Effects of Shallow Weathered Layers," *Zisin* (*Journal *of the Seismological Society of Japan*), **51**: 193–202. (in Japanese with English Abstract)

Yamanaka H, Ohtawara K, Grutas R, Tiglao RB, Lasala M, Narag IC and Bautista BC (2011), "Estimation of Site Amplification and S-wave Velocity Profiles in Metropolitan Manila, the Philippines, from Earthquake Ground Motion Records," *Exploration Geophysics*, **42**(1): 69–79.

Yoshimoto K, Sato H, Kinoshita S and Ohtake M (1993), "High-frequency Site Effect of Hard Rocks at Ashio, Central Japan," *Journal of Physics of the Earth*, **41**(5): 327–335.

Appendix A: Parameters of the earthquakes selected in this study

No.	Event ID	Data yr/mo/da/hr/mn/sc	M_s (M_l)	Long. (°)	Lat. (°)	Depth (km)
1	EQ01	080512144315	6.3	103.82	31.27	14
2	EQ02	080512145417	5.8	103.59	31.26	13
3	EQ03	080512150134	5.5	104.49	31.45	13
4	EQ04	080512151345	(4.7)	103.34	31.07	14
5	EQ05	080512153442	5.8	103.77	31.29	13
6	EQ06	080512154416	(4.6)	103.86	31.34	9
7	EQ07	080512161057	5.5	103.6	31.14	10
8	EQ08	080512162140	5.5	104.28	31.53	11
9	EQ09	080512162612	5.1	104.12	31.4	12
10	EQ10	080512163505	5.2	103.65	31.29	14
11	EQ11	080512163626	(4.2)	103.22	31.05	16
12	EQ12	080512164030	(4.2)	103.48	31.38	12
13	EQ13	080512165039	4.8	105.19	32.24	21
14	EQ14	080512170659	5.2	103.69	31.16	10
15	EQ15	080512173115	5.2	103.56	31.16	10
16	EQ16	080512174224	5.3	104.13	31.48	14
17	EQ17	080512174746	(4.4)	104.05	31.35	25
18	EQ18	080512175655	(3.9)	104.26	31.15	15
19	EQ19	080512182339	5.0	103.48	30.97	9
20	EQ20	080512191101	6.3	103.67	31.26	14
21	EQ21	080512193320	5.0	105.35	32.55	16
22	EQ22	080512201159	4.3	104.24	31.32	15
23	EQ23	080512201348	4.3	103.63	31.39	20
24	EQ24	080512201540	4.9	104.57	31.87	9
25	EQ25	080512203855	4.2	104.26	31.64	20
26	EQ26	080512214053	5.2	103.65	31.02	9
27	EQ27	080512221024	4.6	103.59	31.34	18
28	EQ28	080512221527	4.6	104.77	32.12	19
29	EQ29	080512224606	5.1	105.64	32.72	10
30	EQ30	080512230530	5.2	103.79	31.2	17
31	EQ31	080512230536	5.1	103.42	31.05	14
32	EQ32	080512231658	4.6	103.45	31.15	17
33	EQ33	080512232852	5.1	103.59	31.1	10
34	EQ34	080512235212	(3.7)	104.06	31.22	18
35	EQ35	080513010311	4.6	103.65	31.1	20
36	EQ36	080513012906	4.9	103.68	31.21	24
37	EQ37	080513015432	5.1	103.62	31.26	17
38	EQ38	080513022617	4.1	104.1	31.47	11
39	EQ39	080513024331	4.6	103.84	31.13	20
40	EQ40	080513035319	4.6	103.8	31.19	25
41	EQ41	080513040849	5.8	104.06	31.43	21
42	EQ42	080513044531	5.2	104.55	31.73	20
43	EQ43	080513045127	4.7	105.17	32.33	22
44	EQ44	080513050813	4.5	103.56	31.3	11
45	EQ45	080513064721	4.3	103.66	31.17	9
46	EQ46	080513074618	5.4	103.58	31.34	13
47	EQ47	080513075446	5.2	103.63	31.28	10
48	EQ48	080513082217	4.4	104.03	31.26	12
49	EQ49	080513090759	3.8	103.78	31.29	14
50	EQ50	080513101516	4.3	104.11	31.58	15
51	EQ51	080513103338	4.3	103.81	31.27	14
52	EQ52	080513110038	4.9	103.7	31.21	14
53	EQ53	080513133629	4.4	105.23	32.47	11
54	EQ54	080513143819	4.2	104.04	31.36	13
55	EQ55	080513143951	(4.2)	104.27	31.58	23
56	EQ56	080513150708	6.1	103.42	30.95	14
57	EQ57	080513151916	5.1	105.24	32.35	18
58	EQ58	080513155303	4.7	105.1	32.24	23
59	EQ59	080513162052	4.8	104.05	31.36	17
60	EQ60	080513183642	4.3	103.88	31.25	20

Appendix A: Continued

No.	Event ID	Data yr/mo/da/hr/mn/sc	M_s (M_l)	Long. (°)	Lat. (°)	Depth (km)
61	EQ61	080513211303	4.4	105.2	32.36	17
62	EQ62	080513233038	3.8	104.58	31.05	15
63	EQ63	080514090920	4.2	104.05	31.43	14
64	EQ64	080514095641	4.4	103.8	31.19	13
65	EQ65	080514105437	5.8	103.63	31.34	16
66	EQ66	080514110748	4.3	103.36	31.01	16
67	EQ67	080514135457	4.7	104.24	31.95	15
68	EQ68	080514153217	3.9	104.33	31.86	11
69	EQ69	080514172643	5.1	104.12	31.41	10
70	EQ70	080514180030	4.5	105.15	32.34	12
71	EQ71	080515011723	4.3	103.98	31.43	16
72	EQ72	080515050106	4.8	104.34	31.64	10
73	EQ73	080515100523	3.8	104	31.34	23
74	EQ74	080515201024	4.2	103.87	31.33	10
75	EQ75	080516055547	4.5	104.75	32.26	14
76	EQ76	080516113426	4.9	104.16	31.39	11
77	EQ77	080516132547	5.9	103.45	31.31	14
78	EQ78	080517041652	4.9	103.67	31.21	14
79	EQ79	080517042904	4.4	103.55	31.26	15
80	EQ80	080517083807	4.1	104.37	31.96	12
81	EQ81	080518010824	6.1	105.08	32.2	13
82	EQ82	080519140653	5.5	105.38	32.47	14
83	EQ83	080520015233	5.0	105.07	32.26	15
84	EQ84	080525162147	6.4	105.48	32.55	14
85	EQ85	080527160322	5.3	105.65	32.76	15
86	EQ86	080527163751	5.7	105.7	32.78	15
87	EQ87	080528013510	4.7	105.44	32.66	16
88	EQ88	080605124106	4.8	105.06	32.36	16
89	EQ89	080607142832	4.2	105.51	32.49	15
90	EQ90	080608061428	4.7	105.22	32.43	15
91	EQ91	080619182559	4.4	105.62	32.73	10
92	EQ92	080724035443	5.7	105.63	32.72	10
93	EQ93	080724150928	6.0	105.61	32.76	10
94	EQ94	080801163242	6.2	104.85	32.02	14
95	EQ95	080805174916	6.5	105.61	32.72	13
96	EQ96	080807161534	5.0	104.73	32.12	15

Appendix B: Parameters of stations in the dataset

No.	Station ID	Long. (°)	Lat. (°)	No. of records	V_{s20} (m/s)	Predominant frequency		Average site amplification		
						This study	Wen *et al*., 2011	1.0-5.0 Hz	5.0-10.0 Hz	1.0-10.0 Hz
1	51AXT	104.42	31.46	6	×	2.54	1.61	5.11	2.67	3.76
2	51CXQ	105.93	31.74	4	×	3.81	3.85	9.38	7.43	8.30
3	51GYQ	105.83	32.44	7	Bedrock	10.94	11.76	2.76	3.15	2.98
4	51GYS	105.84	32.15	5	×	8.01	8.33	5.51	10.58	8.32
5	51GYZ	106.10	32.62	6	291	5.22	4.00	7.65	6.65	7.10
6	51HSD	102.98	32.07	28	294	13.09	12.50	7.13	6.79	6.94
7	51HSL	103.26	32.06	33	291	3.96	3.70	10.84	6.82	8.61
8	51JZG	104.32	33.12	24	260	5.18	5.00	15.22	12.74	13.84
9	51JZW	104.21	33.03	23	275	4.00	3.85	9.76	8.03	8.80
10	51JZY	104.25	33.24	27	369	6.93	6.67	6.25	6.39	6.33
11	51LXM	103.34	31.57	60	261	2.98	3.03	17.00	9.16	12.65
12	51LXS	102.91	31.53	36	270	3.86/13.0	3.85/12.5	7.03	6.91	6.96
13	51LXT	103.45	31.56	58	281	13.23	-	4.18	7.88	6.23
14	51MXB	103.85	31.68	13	Bedrock	2.78	-	5.22	3.70	4.38
15	51MXD	103.68	32.04	62	238	2.64	1.35	22.40	7.54	14.16
16	51MXN	103.73	31.58	55	348	2.44	1.96	9.31	5.33	7.10
17	51MZQ	104.09	31.52	4	×	2.44	6.67	2.97	2.24	2.57
18	51PJD	103.41	30.25	7	×	3.03	2.94	20.67	4.07	11.47
19	51PJW	103.63	30.29	9	×	3.66	3.23	12.76	3.27	7.50
20	51QLY	103.26	30.42	17	×	8.64	6.67	7.45	10.02	8.87
21	51SFB	103.99	31.28	6	302	6.59	6.67	2.98	9.10	6.37
22	51SPA	103.64	32.51	38	301	3.96	6.67	6.36	6.27	6.31
23	51WCW	103.18	31.03	9	315	8.64	8.33	4.36	9.26	7.08
24	51XJB	102.37	30.99	16	293	13.04	-	5.75	5.25	5.47
25	51XJD	102.64	30.97	9	297	2.69	-	7.89	6.78	7.27
26	62SHW	104.53	33.66	7	342	8.94	3.57	5.63	6.81	6.29
27	62WIX	104.68	32.95	8	Ourcrop	-	-	2.00	2.00	2.00
28	62WUD	104.99	33.35	25	205	1.51/2.88	1.41/4.76	17.63	9.30	13.02

Note: × means there is no available borehole data for this station; - means the predominant frequency is not evidently to be identified for this station; / means for Station 51LXS and 62WUD there are two obvious predominant frequencies

Appendix C: Parameters of recordings from main shock used for analyzing soil nonlinearity

No.	Station ID	Source-to-site distance				PGA (cm/s^2)			PGV (cm/s)			Predominant frequency F_p		
		D_{Hyp} (km)	D_{Aspt} (km)	D_{Rup} (km)	D_{JB} (km)	EW	NS	Geometric mean	EW	NS	Geometric mean	Weak motion	Strong motion	Weak / Strong
1	51AXT	112.8	75.2	26.2	25.4	289.4	203.4	242.6	29.0	31.3	30.1	2.54	2.73	0.93
2	51CXQ	256.8	167.9	96.8	95.8	184.8	166.9	175.7	22.9	14.2	18.0	3.81	3.76	1.01
3	51GYQ	282.1	164.9	39.2	35.6	-	-	-	-	-	-	10.94	-	-
4	51GYS	265.7	157.3	56.7	55.9	320.4	274.0	296.3	20.5	23.7	22.0	8.01	2.69	2.98
5	51GYZ	313.8	197.1	64.3	59.3	424.4	410.6	417.5	27.5	42.0	34.0	5.22	2.73	1.91
6	51HSD	122.6	128.8	87.2	115.0	102.5	89.8	95.9	6.2	5.3	5.7	13.09	11.72	1.12
7	51HSL	116.6	108.9	70.3	97.1	107.6	142.6	123.9	7.4	9.4	8.3	3.96	3.47	1.14
8	51JZG	250.6	153.0	91.6	119.3	169.8	241.4	202.5	10.9	8.6	9.7	5.18	4.79	1.08
9	51JZW	237.6	144.7	91.2	118.9	128.1	173.6	149.2	9.8	10.0	9.9	4.00	4.05	0.99
10	51JZY	260.9	166.7	105.2	133.2	91.7	100.0	95.8	7.8	7.3	7.5	6.93	6.49	1.07
11	51LXM	62.9	78.1	30.0	51.5	320.9	283.8	301.8	22.4	19.0	20.6	2.98	2.69	1.11
12	51LXS	73.1	117.7	49.3	75.0	221.3	261.7	240.7	9.1	8.8	8.9	3.86/13.0	3.52/8.98	1.09
13	51LXT	61.9	68.2	24.4	43.5	339.6	342.2	340.9	19.1	13.0	15.7	13.23	8.11	1.63
14	51MXB	87.8	60.3	17.3	28.5	306.6	302.2	304.4	27.7	20.4	23.7	2.78	2.78	1.00
15	51MXD	118.1	84.8	44.5	69.4	246.6	206.1	225.5	17.5	33.4	24.2	2.64	2.15	1.23
16	51MXN	72.5	54.2	16.4	27.6	421.1	349.2	383.5	33.3	26.9	29.9	2.44	1.90	1.28
17	51MZQ	89.4	60.7	4.3	1.2	824.6	803.3	813.9	136.3	66.3	95.0	2.44	2.10	1.16
18	51PJD	87.0	174.4	66.0	64.4	195.8	190.3	193.0	19.6	15.5	17.4	3.03	2.78	1.09
19	51PJW	86.1	164.5	75.6	74.5	97.7	101.2	99.4	20.0	10.1	14.2	3.66	3.27	1.12
20	51QLY	68.8	161.1	42.0	40.3	173.7	199.8	186.3	16.5	8.3	11.7	8.64	7.13	1.21
21	51SFB	67.4	60.6	14.7	13.8	558.2	585.7	571.8	85.0	79.1	82.0	6.59	2.73	2.41
22	51SPA	168.0	116.3	83.4	110.7	186.6	131.6	156.7	6.9	8.0	7.5	3.96	3.66	1.08
23	51WCW	22.6	105.2	9.7	16.2	957.3	652.4	790.3	53.4	45.0	49.1	8.64	2.29	3.77
24	51XJB	96.1	182.0	49.8	67.5	67.9	73.8	70.8	4.4	6.5	5.3	2.64	2.78	0.95
25	51XJD	71.3	158.9	28.4	44.9	94.9	132.1	112.0	5.9	9.9	7.7	2.69	2.78	0.96
26	62SHW	313.0	212.4	123.7	151.1	91.4	108.8	99.7	9.2	6.1	7.5	8.94	9.13	0.98
27	62WIX	247.9	134.3	56.9	82.7	142.6	141.1	141.9	11.8	9.1	10.4	-	-	-
28	62WUD	301.5	187.1	76.2	100.1	184.8	163.9	174.1	16.5	13.5	14.9	1.51/2.88	1.22/2.73	1.24

Note: - means no data; / for Station 51LXS and 62WUD there are two obvious predominant frequencies.